Proceedings of ASME Turbo Expo 2025
Turbomachinery Technical Conference and Exposition
GT2025
June 16-20, 2025, Memphis, Tennessee

GT2025-152180

OPERABILITY STUDY WITH SPATIAL RESOLVED TEMPERATURE AND WATER MOLAR CONCENTRATION MEASUREMENTS OF A NEW PRESSURISED OPTICAL MODULAR STAGED COMBUSTOR

Anthony Giles
Cardiff University
Cardiff, UK

Lee Weller
University of Cambridge
Cambridge, UK

Burak Göktepe
Cardiff University
Cardiff, UK

Oussama Chaib
University of Cambridge
Cambridge, UK

Priyav Shah
University of Oxford
Oxford, UK

Ben Williams
University of Oxford
Oxford, UK

Andrew Crayford
Cardiff University
Cardiff, UK

Daniel Pugh
Cardiff University
Cardiff, UK

Simone Hochgreb
University of Cambridge
Cambridge, UK

ABSTRACT

A new optical modular staged combustor has been developed to facilitate the study of the staged combustion of alternative fuels, both liquid and gaseous, at elevated inlet pressures and temperatures. Initial testing to characterize the combustor was carried out at pressures of up to 6 bara, for both premixed and non-premixed methane/air swirling flames with a combustor inlet temperature of 450 K. Exhaust gas analysis together with OH and CH* chemiluminescence was used to evaluate the operability of the combustor and the quenching effect of the secondary air flow for a range of primary and global equivalence ratios. Laser Induced Grating Spectroscopy (LIGS) was used to obtain instantaneous local temperatures of the mixture across the secondary air mixing zone. A previously developed analytic approach was used to extract temperature from the measured signal frequencies within the primary flame brush and secondary mixing region, where both burnt and unburnt gases were present. The development of such modular apparatus specifically to allow for the application of novel optical techniques, such as LIGS, enables the future evaluation of different combustor architectures for unconventional fuels. Additionally, this work further demonstrates the development of the LIGS technique for obtaining measurements within complex high-pressure, turbulent swirling flames.*

Keywords: Staged Combustion, Premixed, Non-premixed, LIGS, Temperature, Spatial, Electrostrictive

NOMENCLATURE

Symbols

ϕ	Equivalence ratio [-]
$\dot{m}$	Mass flow [g s-1]
P	Combustor pressure, absolute [Pa]
T	Temperature [K]

Subscripts

BF	Burner Face
EXH	Exhaust or Combustor Outlet
GLOB	Combustor Overall
LT	Lance Tip
METH	Methane Fuel
PRIM	Primary Air Flow
SEC	Secondary Air Flow

Acronyms

AFT	Adiabatic Flame Temperature
CARS	Coherent Anti-Stokes Raman Spectroscopy
CRZ	Central Recirculation Zone
CW	Continuous Wave
FFT	Fast Fourier Transform
GTRC	Gas Turbine Research Center
HPOC	High-Pressure Optical Chamber
LIF	Laser-Induced Fluorescence
LIGS	Laser-Induced Grating Spectroscopy
MFR	Momentum Flux Ratio
OMSC	Optical Modular Staged Combustor
ORZ	Outer Recirculation Zone
PILOT	Portable In-line LIGS for Optical Thermometry
PIV	Particle Image Velocimetry
TC	Thermocouple

1. INTRODUCTION

A new optical modular staged combustor (OMSC) has been developed for alternate fuel and combustor design research whilst also allowing the study of conventional configurations. The OMSC is installed within the high-pressure optical chamber (HPOC) in operation at the Gas Turbine Research Centre (GTRC) – Cardiff University.

The modular nature of the new combustor allows for the investigation of a variety of alternate architectures: with aviation relevant liquid fuel studies and flameless combustion concepts example areas of intended research. The OMSC configuration used in this work (Fig. 1) comprises of a mixing plenum, burner holder and mounting plate all made from stainless steel. The burner assembly is mounted to an optical and exhaust section, both made from high temperature nickel alloys. The entire combustor is attached to the outlet flange of the HPOC pressure casing. An array of effusion cooling holes are located along the surface of the exhaust and optical section, as well as the burner mounting plate used in this work; which is of a swirl stabilized design previously demonstrated by the authors [1-5].

Assemblies allowing for the placement of secondary air nozzles or large optical windows are located on the four sides of the optical section. These windows facilitate the use of a range of non-intrusive optical techniques, such as chemiluminescence imaging, Laser Induced Fluorescence (LIF), Particle Image Velocimetry (PIV), and Laser-Induced Grating Spectroscopy (LIGS), and potentially, Coherent Anti-Stokes Raman Spectroscopy (CARS). In this work, a range of conditions was specified to map/characterize the stability of the new combustor operating in a staged flame configuration – whilst further appraising the efficacy of LIGS as a new, developmental technique.

The LIGS technique has proven capable of delivering highly accurate and precise temperature [6–10], pressure [11], velocity, and molar concentration measurements in reacting flows [12–16]. A typical LIGS experiment involves the formation of an interference pattern within a control volume formed at the intersection of two crossed, coherent pulsed laser beams. The addition of laser energy to the sample leads to a transient density grating which propagates at the speed of sound, which can be probed using a second continuous wave (CW) beam, which detects the corresponding fluctuations in index of refraction. The CW probe beam is scattered at its own wavelength by the local moving density pattern and detected as a coherent laser beam at the Bragg angle for maximum signal. The modulation frequency of the transient grating can be detected with high accuracy using an oscilloscope, and transformed into the local speed of sound. The intensity of the LIGS signal increases with the local density, so that the technique is particularly suitable for studies at elevated pressure conditions.

The Portable In-line LIGS for Optical Thermometry (PILOT) unit [17] was deployed in this work to obtain, for the first time, LIGS measurements in a pressurized combustor operating with a staged air configuration. The unit was mounted onto a motorized translation stage to allow for spatial mapping within the combustor. For a premixed primary air/methane swirl burner, measurements were collected at several radial locations coinciding with the axial position of the secondary air introduction; with the signals obtained showing evidence of the transition from the central reacting zone to the non-reacting zone within the secondary air jets.

In this paper, the experimental setup used for the elevated pressure benchmarking of the new staged combustor is introduced, detailing the pressure vessel housing the combustor, associated fuel and air control equipment, the chemiluminescence setup, and the details of the PILOT unit to obtain sample LIGS measurements. Initial results from operating the combustor in both premixed and non-premixed configuration are discussed, followed by sample temperature and water vapor molar fraction profiles from the LIGS measurements.

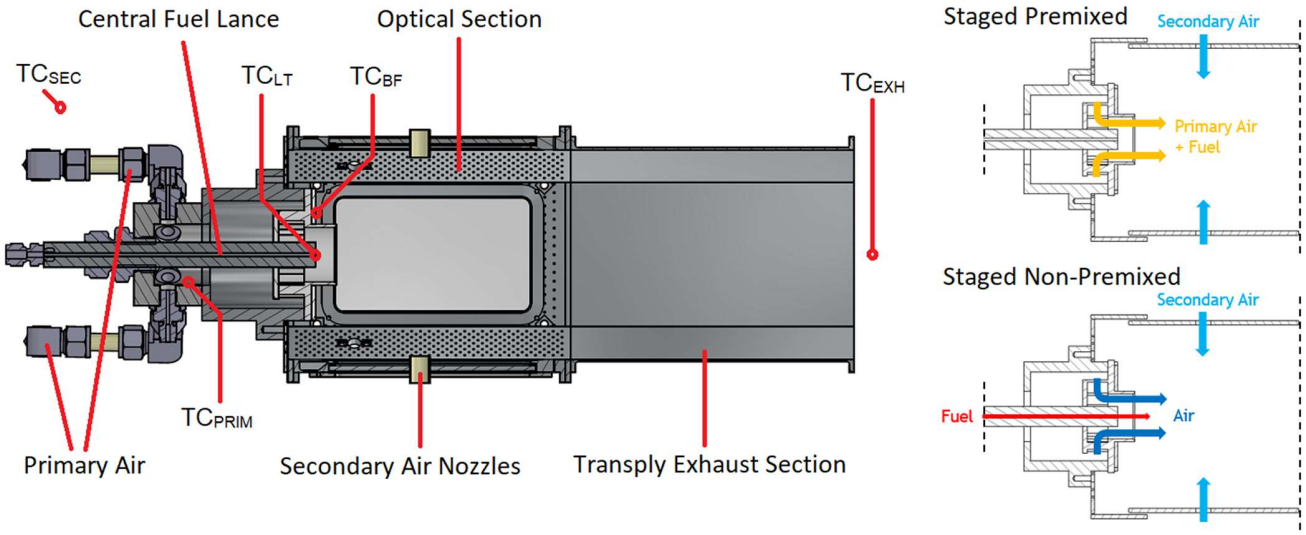

FIGURE 1: SCHEMATIC OF OPTICAL MODULAR STAGED COMBUSTOR, WITH THERMOCOUPLE (TC) LOCATION

2. EXPERIMENTAL METHODS

2.1 High-pressure combustion rig and operating conditions

The optical modular staged combustor (OMSC) is housed in a high-pressure optical chamber (HPOC). Optical access to the combustor was provided both through the HPOC casing and the OMSC by two outer one-inch thick obround Spectrosil 2000 windows, and two inner 4 mm thick rectangular Spectrosil 2000 windows respectively. Pressurization of the rig is achieved utilizing a back pressure control valve. Air was provided by a variable drive speed air compressor, with an air dryer, feeding separate primary and secondary electric preheaters. Micro Motion ELITE Coriolis mass flow meters were used to separately control the primary air flow, secondary air flow, and the methane flow. Additionally, a Bronkhorst M14 mass flow controller was used to meter a constant 0.5 gs^{-1} of the secondary air flow to provide a window purge, in which air is introduced though an array of small holes along the leading edge of each window on the interior of the OMSC.

During testing, the burner was first ignited at a stable atmospheric pressure operating condition. Air and methane mass flow rates were then adjusted to increase the absolute pressure to 0.3 MPa while closing the back pressure valve. To achieve the 0.6 MPa absolute pressure operating condition, the air flows and fuel flows were increased commensurately while further closing the back pressure valve. For the work presented here, a 3D printed Inconel burner insert with a geometric swirl number of 2.0 was used, the dimensions of which are shown in Fig. 2.

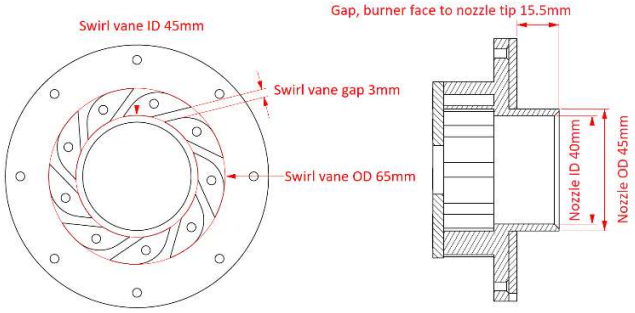

FIGURE 2: DIMENSIONS OF HIGH SWIRL INSERT

A dedicated data acquisition system was used to log the operating conditions during the experiments. Druck PDCR 10/T static pressure transducers were used to measure the pressure within the HPOC. K-type thermocouples were installed at the secondary air entry point to the HPOC and within the plenum of the OMSC to monitor the air delivery temperatures during the experiment. Additional K-type thermocouples were installed at a position in plane and adjacent to the burner face and at the tip of the 18mm diameter bluff body lance within the swirl insert (note: the lance tip thermocouple was replaced for the non-premixed experiments by a 5 mm orifice used for fuel injection). An N-type thermocouple was positioned centrally at the exit of the HPOC to provide an exhaust gas temperature.

An equal area probe (9 holes) was used to extract a sample of the exhaust gas stream in accordance with ISO 11042 [18], and was located at a point approximately 10 diameters downstream of the combustor exit. Sample conditioning was achieved by actively cooling the sample probe to 433 K, and then maintaining the sample line, filter, distribution manifolds and system pump at this temperature to deliver products to the analysis suite. Total NO_X concentrations were measured hot and wet (to avoid water absorption losses) and quantified using a heated vacuum chemiluminescence analyzer (Signal Instruments 4000VM, calibrated in the range 0 – 40.2 ppmV), with the data normalized to equivalent dry conditions prior to presentation. An additional sample was directed to a chiller (to reduce the molar water concentration below 1%) before downstream CO, CO_2 and O_2 measurements were made using a combination of nondispersive infrared and paramagnetic analyzers (Signal instruments 9000MGA). These were calibrated in the respective ranges of zero to full scale (FS), where FS is 897 ppm, 8.99% and 22.94%, all based on molar concentrations.

The configuration of the OMSC chosen for this experimental work included the addition of three secondary air nozzles in both the top and bottom window plates. These inlet nozzles were each 13.5 mm in diameter, and positioned axially such that secondary air jets were introduced across a plane 60 mm from the burner exit. To ascertain the proportion of air that entered through the nozzles and the separate effusion cooling hole locations, isothermal flow tests were carried out. The distribution of the total secondary air flows (excluding the separately metered window purge air) is indicated in Fig. 3.

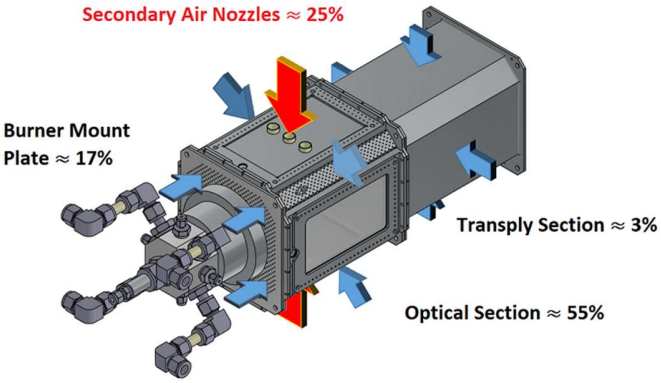

FIGURE 3: SECONDARY AIR (RED) & EFUSION COOLING (BLUE)

For the experimental work presented here, a target air preheat temperature of 475 ± 25 K was chosen, although this was difficult to maintain in practice due to the low value of primary air flows, and the large variation in secondary air flow between conditions. Methane flow rates of 0.68 gs^{-1} and 1.36 gs^{-1} were used for the 0.3 MPa and 0.6 MPa conditions respectively; the fuel flow rates were set to maintain a constant power scaling for the pressurized combustion of ≈ 113 kW/MPa, essentially maintaining combustor velocity fields and residence time. The target primary and secondary air flow values used for each of the

test conditions are shown in Table 1. Additionally, following established methodology [19] and an estimated momentum flux ratio (MFR) for the primary / secondary air nozzle flows based upon the proportional flow of secondary air into the combustor is included. The MFR is a parameter known to significantly affect the mixing characteristics and combustion efficiency.

TABLE 1: AIR FLOW RATES AT OPERATIONAL CONDITIONS

		GLOBAL EQUIVALENCE RATIO ϕ_{GLOB}			
		0.55	**0.40**	**0.30**	
PRIMARY REGION EQUIVALENCE RATIO ϕ_{PRIM}	**2.00**	5.860 gs^{-1}			$\dot{m}_{PRIM}$
		15.45 gs^{-1}	23.44 gs^{-1}	33.21 gs^{-1}	$\dot{m}_{SEC}$
		9.3	21.3	42.8	MFR
	2.25	5.209 gs^{-1}			$\dot{m}_{PRIM}$
		16.10 gs^{-1}	24.09 gs^{-1}	33.86 gs^{-1}	$\dot{m}_{SEC}$
		12.5	27.9	55.1	MFR
	2.50	4.688 gs^{-1}			$\dot{m}_{PRIM}$
		16.62 gs^{-1}	24.61 gs^{-1}	34.38 gs^{-1}	$\dot{m}_{SEC}$
		16.1	35.2	68.7	MFR

For both non-premixed and premixed flame configurations, experiments were carried out at a combustor pressure of 0.3 MPa at each of the nine test conditions shown in Table 1; the equivalence ratio of the primary zone (Φ_{PRIM}) set at 2.00, 2.25 and 2.50. For each primary equivalence ratio value, the total secondary air flow was varied such that the global combustor equivalence ratios values (Φ_{GLOB}) were 0.30, 0.40 or 0.55.

At the 0.6 MPa pressure a single operational point was evaluated, with a Φ_{PRIM} of 2.25 and a Φ_{GLOB} of 0.40 chosen. In order to keep the bulk volumetric flow rates constant, the aforementioned power scaling was applied with the flow rates doubled to reflect the pressure increase.

3.2 CH* and OH* Chemiluminescence

The chemiluminescence system used in the study has been described previously [20]. Chemiluminescence images of the excited methylidyne (CH*) and hydroxyl (OH*) radicals at wavelengths of 431 nm and 310 nm respectively were used as a marker of flame front location and localized heat release rate. A high-speed camera (Phantom v1212 CMOS camera) coupled to a high-speed image intensifier (SIL40HG50) and a UV lens (78 mm focal length, F-stop = f/11), together with narrow band pass filters (center wavelengths of 430 nm and 315 nm) was used to capture the CH* and OH* signals.

Note that the chemiluminescence images of the premixed operating conditions were not taken at the same time as the data obtained by the LIGS PILOT system, as the experiments were repeated without the laser system in place. For the images taken, the setup allowed for a resolution of approximately 5 pixels mm^{-1}, with the focus of the image plane aligned to the center of the burner exit nozzle. The optical access of the staged combustor within the HPOC permitted respective view fields of 100 mm in the radial and 120 mm in the axial direction. For each of the experimental conditions the chemiluminescence results comprise of 2000 CH* and OH* images recorded at a rate of 4 kHz (sample time = 0.5 s). An intensifier gain value of 2 and a gate setting of 10 μs was used for the CH* and OH* for all the premixed results. For the non-premixed measurements, the same gain and gating sections were used for the OH* results, whilst a gain value of 1 and gating of 100 ns was used for the CH* emissions. After a background correction was applied, an averaged image was produced, from which normalized planar representations of the CH* and OH* chemiluminescence intensity distributions were generated using a modified open-access Abel inversion algorithm [21], assuming cylindrical symmetry.

3.3 PILOT System

The PILOT unit was used to obtain LIGS measurements for the range of premixed operating conditions previously defined. The design and characterization of the PILOT system has been previously discussed [17]. The setup is capable of obtaining time resolved tracer-free LIGS measurements at repetition rates of up to 400 Hz. Pump beams (from a Nd:YAG Quantel Merion C laser) are produced at 1064 nm, with an adjustable energy of up to 35 mJ per beam delivered over a 7 ns pulse duration. A probe beam at 532 nm, with an adjustable power of up to 18 W, was produced from a Coherent Verdi V-18 laser. The wavelength and energy of the system allows for tracer-free electrostrictive and water-thermal LIGS measurements.

A 2-axis motorized translation stage was used to mount the PILOT unit as well as a detection rail, which contained the signal detection optics for the PILOT unit. This allowed for the complete system to be remotely operated and moved to obtain measurements from different locations within the combustor, while ensuring that the PILOT delivery and detection optics would not be affected by any rig vibrations during operation. To improve the SNR ratio of the LIGS signals, a spatial filter was introduced onto the detection rail to reject reflected light from the HPOC windows. The spatial filter consisted of a pin hole (250 μm) placed at the mid-point between two lenses, each with a focal length f = 100 mm and separated by 200 mm. A Hamamatsu H10721-20 photomultiplier tube was used to collect the LIGS signals, which were digitized by a Picoscope 6402 oscilloscope (8-bit channel at 500 MHz) from Pico Technology. A photodiode (Thorlabs DET210) was used for the detection of the pump beam and triggering of the oscilloscope for the acquisition of the LIGS signals. The signals were acquired at 10 Hz for a total of 100 seconds at each test point.

The raw captured LIGS signal comprises of multiple single shots (typically 1260), which are individually filtered before applying a Fast Fourier Transform (FFT) to obtain a power spectrum. From this, the thermal and electrostrictive character of the signal can be ascertained based upon the dominant frequencies and their relative magnitudes, with further analysis allowing for the subsequent calculation of a temperature value.

3. RESULTS AND DISCUSSION

3.1 Premixed Pressurized Combustion Results

Fig. 4 displays the combined results and measured operating conditions for the matrix of premixed 0.3 MPa test points studied in this work (with Φ_{PRIM} values of 2.00, 2.25 and 2.50; Φ_{GLOB} values of 0.55, 0.40 and 0.30).

Average values of the measured flow rates, temperatures and combustor pressure (calculated for a period of 5 minutes of steady operation) as well as average emission data for each test point are shown alongside the Abel inverted CH* and OH* chemiluminescence images. For reference, the corresponding color scale for the minimum and maximum intensities of the normalized chemiluminescence images is included in Figs 5 and 7. Typical combined measurement uncertainties (systematic and experimental) for the flow rates during a 5 minute steady operation period were found to be ≈ 1% for the air flows and ≈1.5% for the fuel flow. Total uncertainties for inlet air temperatures was found to be ≈3 K and for the measured pressure values < 0.01 MPa, The total uncertainties in the measured exhaust gas, burner face and lance tip temperatures was found to be ≈4 K.

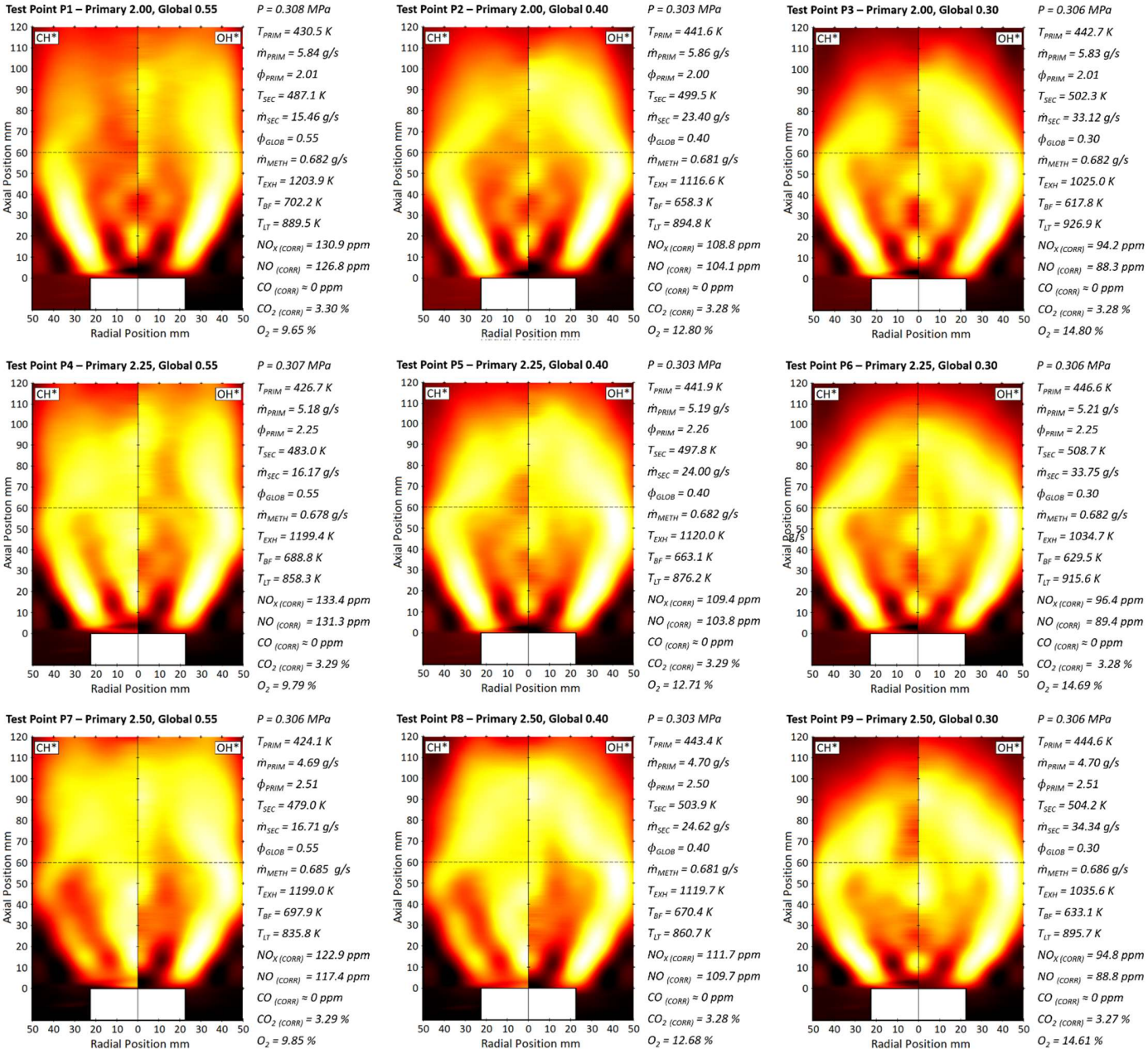

FIGURE 4: ABEL INVERTED CH* AND OH* CHEMILUMINESCENCE IMAGES AT 0.3 MPA, PREMIXED OPERATING CONDITIONS.

The CH* and OH* images shown in Fig. 4 exhibit similar overall flame shapes for all of the operating conditions tested, with a conical flame position surrounding a central recirculation zone (CRZ) and zero axial velocity shear layer. Two outer recirculation zones (ORZ) appear to be situated radially around the exit nozzle. Both of these structures are typical for this premixed swirl burner configuration, and have been identified in previous work [5]. The introduction of secondary air jets at the 60 mm axial position can be seen to disrupt the conical flame structure, with the opposing jets resulting in the narrowing of the flame at higher axial positions. This becomes more distinct in the images for test points P3, P6 and P9 (Φ_{GLOB} value = 0.30), corresponding to the conditions with the highest secondary air flows and highest calculated MFR values.

Examining the location of peak CH* intensity for the conditions investigated (indicated by the brightest position in the left halves of the images of Fig. 4), it can be seen that the reduction in reactivity from increasing Φ_{PRIM} moves the location for both CH* and OH* formation away from the burner exit; this is corroborated by a reduction in both the lance tip and burner face temperatures measured. The measured exhaust temperatures and corrected NO_X values do not show any significant variation with changes in Φ_{PRIM} over the range measured; however, both temperature and NO_X can decrease with the increased dilution introduced as Φ_{GLOB} is lowered. An increase in secondary air flow, and a corresponding reduction in Φ_{GLOB} has the effect of reducing both the measured exhaust gas temperature and corrected NO_X values. This may not be related to any change in the peak flame temperature within the reaction zone, but a result of the additional dilution.

Fig. 5 displays the results for the 0.6 MPa premixed operation condition (test point P10), with the mass flows and combustor pressure effectively double the values used for test point P5 (shown in Fig. 4). The experimental uncertainties for the measured values for 0.6 MPa operation were found to be comparable to that seen for the 0.3 MPa conditions.

Visually, the chemiluminescence images for the 0.6 MPa premixed combustion case exhibit the same general structure as the comparable 0.3 MPa condition. However, there is an intensification in the detected CH* emission, possibly due to the increase in power density caused by the scaling with pressure. Both an increase in measured exhaust gas temperature and corrected NO_X emissions are additional evidence for the reaction intensification when comparing test point P10 to P5. The higher exhaust gas temperature also leads to an increase in temperatures measured at the lance tip, due to the presence of these hotter gases within the CRZ.

For all the premixed results presented in Figures 4 and 5, the measured CO values were below that detectable by the gas analysis system. Yet it would be expected that significant CO formation occurs within the fuel rich primary combustion zone. The introduction of the secondary air apparently allows for sufficient mixing for complete combustion to occur before the gases exit the combustor; with there being sufficient residence time, temperature and excess air to further oxidize the CO.

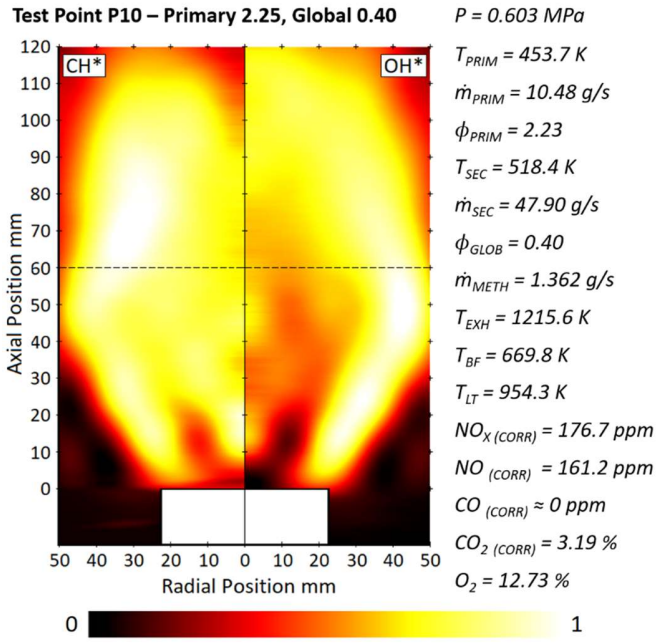

FIGURE 5: 0.6 MPa PREMIXED OPERATION CONDITION, ABEL INVERTED CH* AND OH* CHEMILUMINESCENCE IMAGES

3.2 Non-premixed Pressurized Combustion Results

The combined results and measured operating conditions for the case of a non-premixed flame at 0.3 MPa test points are shown in Fig. 6. Again the same Φ_{PRIM} values (2.00, 2.25 and 2.50) and Φ_{GLOB} values (0.55, 0.40 and 0.30) are presented.

For the non-premixed flame results, the typical combined uncertainties (systematic and fluctuations) were again calculated for a 5 minute period over which steady operation was maintained. The uncertainty in the air flow values were found to be ≈ 1%, and the fuel flow values ≈1.5%. Total uncertainties for inlet air temperatures was found to be ≈3K and for the measured pressure values < 0.01 MPa. For the exhaust gas temperature there was significant variation in the recorded values over the sampling period (particularly for the carbon monoxide measurements), possibly due to the non-premixed primary flame zones being more unstable than that of the comparable premixed test points. Typical total uncertainties in the measured exhaust gas temperatures were ≈10 K, and ≈4 K for the burner face.

The CH* and OH* images for the 0.3 MPa test points shown in Fig. 6 all demonstrate a significantly different flame shape to the equivalent premixed conditions. With the fuel now entering the combustion zone separately through the centrally located lance, the strength of the CRZ is diminished and as such the flame front and heat release locations are more centrally positioned (indicated by the high intensity regions in the CH* and OH* images).

For a given Φ_{PRIM} value, the effect of reducing Φ_{GLOB} from 0.55 to 0.40 results in the extra air flow shifting the average flame position away from the combustor wall and towards the

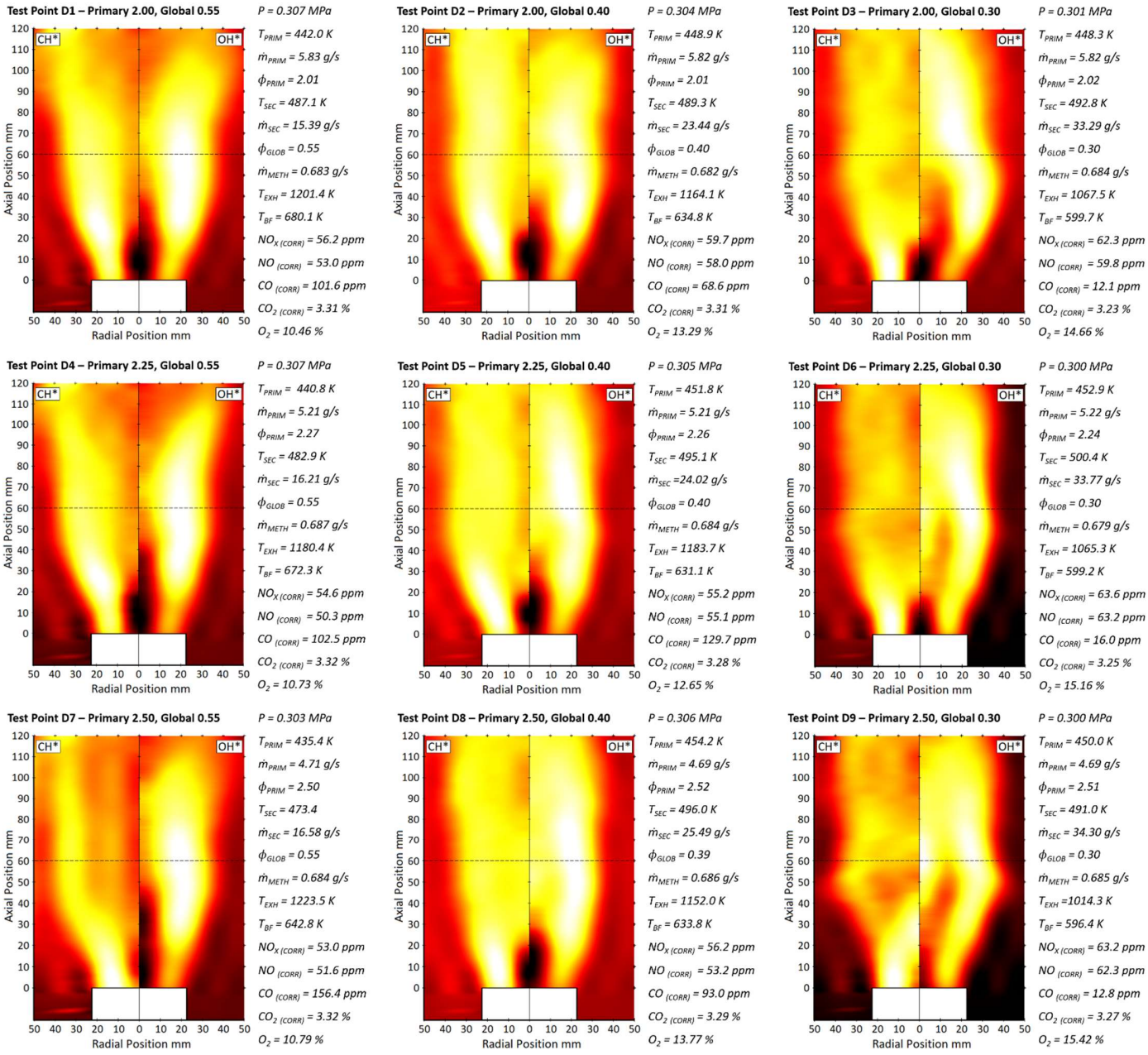

FIGURE 6: 0.3 MPa NON-PREMIXED OPERATING CONDITIONS, ABEL INVERTED CH* AND OH* CHEMILUMINESCENCE IMAGES

center axis. From the CH* images, it appears that a further reduction in Φ_{GLOB} from 0.40 to 0.30 results in the secondary air jets disrupting the center fuel jet and possibly reducing the axial momentum of the primary flame zone, improving the fuel mixing and possibly intensifying the primary combustion zone and increasing peak temperatures. It is possible that higher peak temperatures may explain the measured increase in corrected NO_X with the reduction in Φ_{GLOB}, even though it would be expected that the extra dilution would reduce NO_X in a similar manner to how both the corrected CO and measured exhaust temperature were seen to decrease.

The recorded CO emission values for test points D4 and D5 do not follow the typical trend seen for the premixed results; with the corrected CO values generally reducing as the secondary air flow is increased. However, as previously mentioned there was significant fluctuation seen in the recorded CO measurements and as such the average values may not be representative.

The results for the 0.6 MPa non-premixed flame operation condition (test point D10), are shown in Fig. 7. The mass flow

rates and combustor pressure conditions for test point D10 are effectively double the values used for test point D5 shown in Fig. 6. As before, the experimental uncertainties in the measured values for 0.6 MPa condition were found to be equivalent to that seen at the 0.3 MPa pressure.

The intensity distributions for both the CH* and OH* chemiluminescence images for the 0.6 MPa non-premixed combustion case (D10, shown in Fig. 7), correspond to that of the same 0.3 MPa condition (D5) shown Fig. 6. The increase in power density caused by the scaling of both the fuel and air flows with pressure resulted in an increase in both the measured exhaust gas and burner face temperatures, even though the corrected NO_X emissions for D10 are comparable to that of D5. It is noticeable that the corrected CO emissions measured for the 0.6 MPa test point D10 are higher than that seen in any of the 0.3 MPa test points, and almost double that of the equivalent test condition D5. This suggests that the increase in pressure may have reduced the effectiveness of the mixing of the fuel with the primary combustion air.

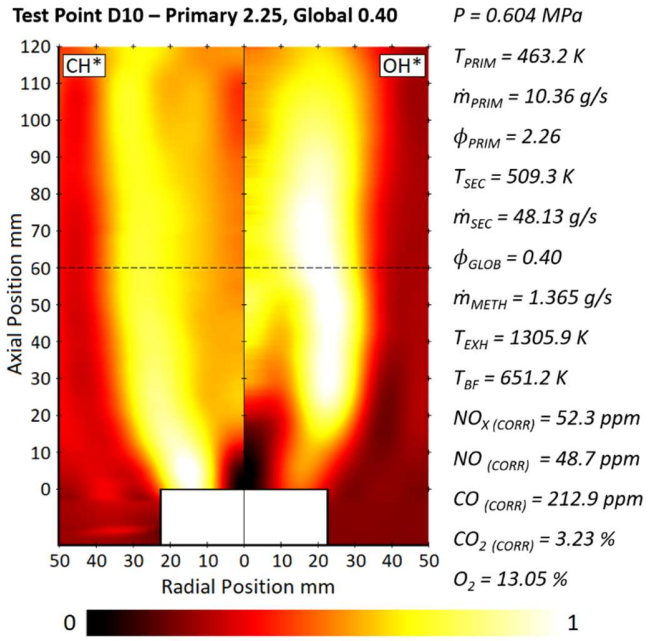

FIGURE 7: 0.6 MPa NON-PREMIXED OPERATION CONDITION, ABEL INVERTED CH* AND OH* CHEMILUMINESCENCE IMAGES

Comparing the results obtained for all of the non-premixed flame cases to that of the premixed flame cases discussed previously, it can be seen that there are no substantial differences in the measured exhaust gas and burner face temperature; with the respective ranges for the 0.3 MPa premixed cases being 1025 K< T_{EXH} < 1204 K and 618 K< T_{BF} < 702 K, and for the 0.3 MPa non-premixed cases 1014 K< T_{EXH} < 1224 K and 596 K< T_{BF} < 680 K. For all comparable operating conditions the burner face temperatures and NO_X emissions are seen to be higher when operating in a premixed configuration, suggesting that the separate introduction of fuel in the non-premixed cases reduces the peak flame temperatures due to an additional mixing delay in the primary zone. Some of the non-premixed cases are found to have a higher exhaust gas temperature than the corresponding premixed test point, possibly due to an elongation of the flame towards the combustor exit resulting in the combustion products being less uniformly mixed in the non-premixed cases; and the centrally located exhaust gas thermocouple not providing a representative reading. The measured CO values for the premixed combustion conditions presented in Figs. 6 and 7 are significantly higher than that previously seen in the premixed test points. From these results it can be surmised that staged combustion, with either a premixed or non-premixed primary flame zone, cannot match the low emission results seen with non-staged lean premixed technologies [1]. Aero-engines predominantly operate with staged combustion systems due to their improved operability (ignitability and flame stability over a greater operational range). For hydrocarbon fueled power generation, staged combustion is regarded as an outmoded concept; however, it has been shown to have advantages for alternative fuels such as hydrogen and ammonia [3, 22].

3.3 LIGS Measurements for Premixed Combustion Testing

Spatially resolved data captured utilizing the PILOT system is presented here for the three 0.3 MPa conditions with a Φ_{PRIM} of 2.25; Φ_{PGLOB} ratios of 0.55 (P4), 0.40 (P5) and 0.30 (P6). Signals were obtained at an axial distance of 60 mm from the burner, corresponding to the location of the secondary air jets, for radial positions of 0 to 50 mm. The configuration of the PILOT system [17] provided an effective spatial resolution of 6 mm in the radial direction and 0.3 mm in the axial direction (with a 0.3 mm resolution in the 3rd axis).

Fig. 8(a) shows color camera images for one half of the OMSC for the three test cases, P4-P6. For all three conditions, outward flow from the burner exit nozzle (ID = 40 mm) forms a conical flame structure encompassing a CRZ and a shear layer characterized by zero axial velocity. Beyond the outer shear layer, an ORZ develops near the walls, containing regions of combustion products, entrained reactants, and their mixtures.

Fig. 8(b) shows normalized single-shot (grey) and averaged LIGS signals for three radial positions (0 mm - red, 30 mm - green and 50 mm - blue) for test points P4-P6. Using FFT analysis, power spectra can be produced and a dominant frequency (or frequencies) extracted. The characteristic signals for the positions across the flame region were found to be similar to that seen in previous work [23] with the thermal and electrostrictive signals being at a location of 0 mm and 50 mm, respectively. The LIGS signals were analyzed using a k-means clustering to identify dominant spectral features through the identification and segregation of similar signals, grouping the data by signal type and allowing for the determination of their relative proportion. Further details of the analysis methodology is described in previous work [24]. Frequencies and ratios extracted from LIGS signals were used to characterize the temperature and water vapor profiles, respectively [25]. For each

test condition, the dominant cluster is highlighted (i.e., the one characterized by the highest number of instantaneous signals) at a given spatial location (0 mm - red, 30 mm - green and 50 mm - blue). The instantaneous single-shot signals in the clusters are depicted in grey, and their corresponding mean (cluster centroid) is drawn in solid color. Depending upon the location within the flame, the LIGS spectra can take the form of either hot thermal combustion products signature, electrostrictive air signature, or a complex combination of both dictated by local mixing.

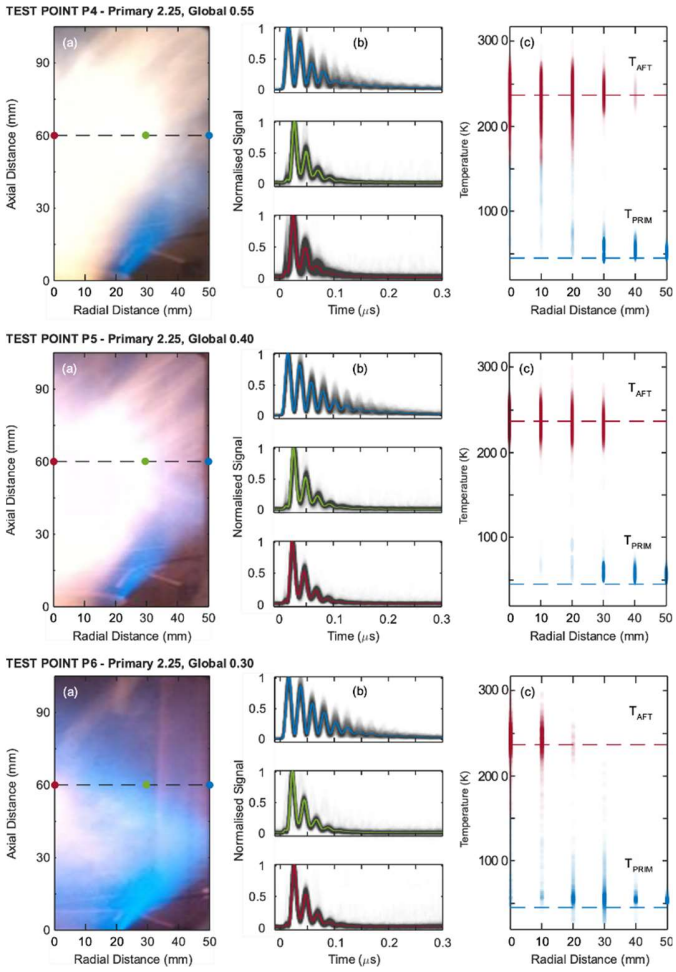

FIGURE 8: (A) VISIBLE CAMERA IMAGE, LOCATING THE MEASUREMENTS AT AXIAL LOCATION 60 MM, (B) EXAMPLE LIGS SIGNALS FOR DIFFERENT RADIAL LOCATIONS AND (C) TEMPERATURE PROFILES AS A FUNCTION OF RADIAL LOCATION AT A FIXED AXIAL LOCATION OF 60 MM FOR THE TEST CASES P4-P6.

Fig. 8(c) shows the calculated radial temperature profiles (from the frequency measurements) at the axial location of 60 mm for the three cases under investigation. The colors indicate predominantly thermal (red) or electrostrictive (blue) LIGS signatures respectively. The intensity of the symbol color is proportional to the normalized peak power spectrum intensity of each 1000-shots. The lowest temperatures are around 450 K, a value which equates to the inlet temperature for the primary air (T_{PRIM} dashed blue line). The mean calculated temperatures of all three cases are consistent with the adiabatic flame temperature (T_{AFT} dashed red line) for a premixed methane-air flame at 0.3 MPa with a preheat temperature of 450 K. Previous studies demonstrated that the ratio of the second to the first peak intensities in LIGS signals correlates with molar fraction of water [25]. This phenomenon arises from the energy absorbed by water vapor influencing the second peak, while the magnitude of first peak results from electrostrictive effects. The ratio is employed to determine instantaneous water molar fractions under various combustion conditions, providing critical insights into the combustor's performance.

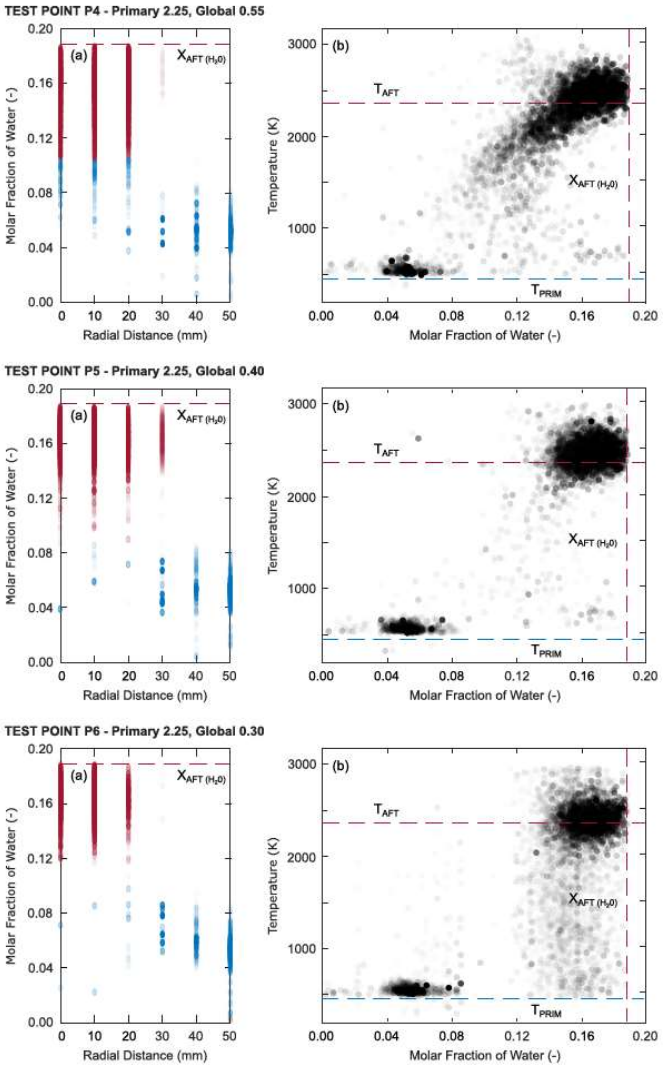

FIGURE 9: (A) MOLAR FRACTION OF WATER AS A FUNCTION OF RADIAL LOCATION AND (B) TEMPERATURE VERSUS MOLAR FRACTION OF WATER AT A FIXED AXIAL LOCATION OF 60 MM FOR THE TEST CASES P4-P6.

Fig. 9(a) shows the calculated radial molar fraction of water profiles (from the signal ratio measurements) at the axial location of 60 mm for the three cases under investigation. The colors indicate predominantly thermal (red) or electrostrictive (blue) LIGS signatures, respectively. The intensity of the symbol color is proportional to the normalized peak power spectrum intensity of each 1000-shots. For the conditions investigated, the highest calculated water molar fraction under adiabatic conditions is $X_{H20\ (AFT)} = 0.188$, and indicated by the horizontal dashed red lines in Fig. 9(a) and the vertical dashed red lines in Fig. 9(b). For all three test conditions, it can be seen that in the central flame locations (radial position up to 30 mm) the calculated water vapor concentrations indicate a high proportion of combustion products, likely being concentrated within the CRZ. The lowest values of the calculated water vapor concentrations are seen at higher radial positions and are non-zero (~0.04), probably due to mixing between incoming reactants and products in the ORZ, where these ratio values were measured.

Fig. 9(b) shows the calculated temperatures versus molar fraction of water for all radial locations at the axial location of 60 mm for the three cases under investigation. An increase in Φ_{PGLOB} appears to be reflected by a change in the temperature versus water molar fraction distribution, which can possibly be related to the MFR values and secondary jet mixing. At a Φ_{PGLOB} value of 0.55 (test point P4) the relatively low momentum secondary air readily interacts with the hot region of the flame, with there being a wide range of both molar water concentrations and temperatures. Test point P5, in which the secondary air has been increased to produce a 0.40 Φ_{PGLOB} value, seems to result in a reduction in the number of recorded signals representing intermediate temperature and molar water concentrations. For test point P6 ($\Phi_{PGLOB} = 0.3$), there is evidence of high molar water fraction products at the range of calculated temperatures from T_{SEC} to T_{AFT}. This suggests that through reducing Φ_{PGLOB} and increasing the secondary air flow (and MFR), there is likely a change in the flow and flame structure within the combustor.

Uncertainties for both the molar fraction of H_2O and the temperature values calculated from the LIGS measurements are related to the experimental setup as well as assumptions made and arising from the post-processing methodology used. The effect of changes in the experimental operating conditions on the LIGS signal was monitored during the data collection process, and when required, alignment of the optical system was optimized to ensure sufficiently high signal-to-noise ratio LIGS signals were collected. The temperature derived from LIGS signals is dependent on the gas composition, and specifically the relationship between the mean molar mass and the ratio of specific heats. For well mixed and homogeneous mixtures, the variation in these parameters is small, limiting the error in the calculated temperature; with previous work demonstrating a measurement precision in the range of 0.1 to 1.0% for the LIGS technique [26]. The k-means clustering technique employed in this work, and the manner in which the signals are segregated effectively allows for a sensible evaluation of the gas composition, further minimizing this source of uncertainty.

4. CONCLUSION

A new optical modular staged combustor has been demonstrated at elevated inlet pressures and temperature conditions for both premixed and non-premixed methane/air swirling flames. The operability of the combustor, with varied addition of secondary air flow, was evaluated through the use of OH* and CH* chemiluminescence together with exhaust emission analysis.

LIGS was utilized to obtain measurements within a staged combustor for the first time, providing spatially resolved temperature and water concentration data for academic and industrial use. A k-means processing methodology was employed to process the spatially resolved electrostrictive and thermal LIGS signals. Near to the center axis of the premixed staged swirl burner; average temperatures were calculated that corresponded to the adiabatic flame temperature for the mixture, and water concentration values approached that of the theoretical maximum. Moving out from the center there is a reduction in both the measured temperature and water concentration, eventually reducing to that of the secondary air.

The successful evaluation of the new optical modular staged combustor will facilitate future research into burner development and fuel blend suitability.

ACKNOWLEDGEMENTS

All research (i.e. facility, consumable and staff time) was funded during this work under EPSRC UK Award EP/T030801/1 within the LIGS project. Thanks to Daniel Eakins and David Chapman for loan of the Verdi V-18 laser from Coherent. The dataset associated with this article is available from the corresponding author on request.

The experimental datasets, images, details of the combustor geometry and initial isothermal PIV results have been made available to facilitate the development and validation of computer models (DOI link 10.17035/cardiff.28342706).

REFERENCES

[1] Runyon, J., Marsh, R., Bowen, P., Pugh, D., Giles, A. and Morris, S. “Lean methane flame stability in a premixed generic swirl burner: Isothermal flow and atmospheric combustion characterization.” *Experimental Thermal and Fluid Science* Vol. 92 (2018): pp. 125–140.

[2] Pugh, D., Bowen, P., Crayford, A., Marsh, R., Runyon, J., Morris, S. and Giles, A. “Catalytic influence of water vapor on lean blow-off and NOx reduction for pressurized swirling syngas flames.” *Journal of Engineering for Gas Turbines and Power* Vol. 140 No. 6.

[3] Pugh, D., Bowen, P., Valera-Medina, A., Giles, A., Runyon, J. and Marsh, R. “Influence of steam addition and elevated ambient conditions on NOx reduction in a staged premixed swirling NH3/H2 flame.” *Proceedings of the combustion institute* Vol. 37 No. 4 (2019): pp. 5401–5409.

[4] Pugh, D., Bowen, P., Marsh, R., Crayford, A., Runyon, J., Morris, S., Valera-Medina, A. and Giles, A. "Dissociative influence of H2O vapour/spray on lean blowoff and NOx reduction for heavily carbonaceous syngas swirling flames." *Combustion and flame* Vol. 177 (2017): pp. 37–48.

[5] Marsh, R, Runyon, J, Giles, A, Morris, S, Pugh, D, Valera-Medina, A and Bowen, P. "Premixed methane oxycombustion in nitrogen and carbon dioxide atmospheres: measurement of operating limits, flame location and emissions. *Proceedings of the Combustion Institute*." Proceedings of the Combustion Institute Vol. 36 No. 3 (2017): pp. 3949–3958.

[6] Kiefer, J. and Ewart, P. "Laser diagnostics and minor species detection in combustion using resonant fourwave mixing." *Progress in Energy and Combustion Science* Vol. 37 No. 5 (2011): pp. 525–564.

[7] Gutfleisch, M, Shin, DI, Dreier, T and Danehy, PM. "Midinfrared laser-induced grating experiments of C2H4 and NH3 from 0.1–2 MPa and 300–800 K." *Applied Physics B* Vol. 71 No. 5 (2000): pp. 673–680.

[8] Stevens, R and Ewart, P. "Single-shot measurement of temperature and pressure using laser-induced thermal gratings with a long probe pulse." *Applied Physics B* Vol. 78 No. 1 (2004): pp. 111–117.

[9] Stampanoni-Panariello, A., Kozlov, D.N., Radi, .PP. and Hemmerling, B. "Gas phase diagnostics by laser-induced gratings I. Theory." *Applied Physics B* Vol. 81 No. 1 (2005): pp. 101–111.

[10] Stampanoni-Panariello, A., Kozlov, D.N., Radi, P.P. and Hemmerling, B. "Gas-phase diagnostics by laser-induced gratings II. Experiments." *Applied Physics B* Vol. 81 No. 1 (2005): pp. 113–129.

[11] Wu, Y., Zhuzou, M., Zhao, T., Ding, P., Sun, S., Wang, J., Liu, Z. and Hu, B. "Gas-phase pressure measurement using femtosecond laser-induced grating scattering technique." *Optics Letters* Vol. 47 No. 7 (2022): pp. 1859–1862.

[12] Brown, M.S. and Roberts, W.L. "Thermometry in pressurized sooting flames using laser-induced gratings." *Optical Technology in Fluid, Thermal, and Combustion Flow III*, Vol. 3172 (1997): pp. 492–503. SPIE.

[12] Sahlberg, A.-L., Hot, D., Kiefer, J., Aldén, M. and Li, Z. "Mid-infrared laser-induced thermal grating spectroscopy in flames." Proceedings of the Combustion Institute Vol. 36 No. 3 (2017): pp. 4515–4523.

[14] De Domenico, F., Guiberti, T.F, Hochgreb, S., Roberts,W.L. and Magnotti, G. "Temperature and water measurements in flames using 1064 nm Laser-Induced Grating Spectroscopy (LIGS)." *Combustion and Flame* Vol. 205 (2019): pp. 336–344.

[15] Hayakawa, A., Yamagami, T., Takeuchi, K., Higuchi, Y., Kudo, T., Lowe, S., Gao, Y., Hochgreb, S. and Kobayashi, H. "Quantitative measurement of temperature in oxygen enriched CH4/O2/N2 premixed flames using Laser Induced Thermal Grating Spectroscopy (LITGS) up to 1.0 MPa." *Proceedings of the Combustion Institute* Vol. 37 No. 2 (2019): pp. 1427–1434.

[16] Hot, D., Sahlberg, A.L., Aldén, M. and Li, Z. "Mid-infrared laser-induced thermal grating spectroscopy of hot water lines for flame thermometry." *Proceedings of the Combustion Institute* Vol. 38, No. 1 (2021): pp 1885-1893.

[17] Shah, P., Le Page, L. M., and Williams, B. A., "Development and Characterization of PILOT: A Transportable Instrument for Laser-Induced Grating Spectroscopy," *Opt. Express*, Vol. 31 No. 4 (2023): pp. 5872–5881.

[18] "British Standard ISO 11042-1:1996, Gas turbines. Exhaust gas emission, Measurement and evaluation," British Standards Institution, U.K., 1996.

[19] U.S. Department of Energy-National Energy Technology Laboratory (NETL); Smith, Lance; Karim, Hasan; Etemad, Shahrokh; and Pfefferle, William C., "The Gas Turbine Handbook" *Engineering Faculty Book Gallery.* 3. (2006).

[20] Runyon, J., Marsh, R., Sevcenco, Y., Pugh, D., Morris, S. "Development and commissioning of a chemiluminescence imaging system for an optically-accessible high-pressure generic swirl burner" *7th European Combustion Meeting* (2015) Paper P3-29.

[21] Killer, C., "Abel Inversion Algorithm", https://www.mathworks.com/matlabcentral/fileexchange/43639-abel-inversion-algorithm (2013) Accessed 01/12/2015.

[22] Cecere, D., Giacomazzi, E., Di Nardo, A., Calchetti G. "Gas Turbine Combustion Technologies for Hydrogen Blends" *Energies* Vol 16, 6829 (2023): pp. 1-29.

[23] Weller, L., Shah, P., Giles, A., De Domenico, F., Morris, S., Williams, B. A. and Hochgreb, S., "Spatial Temperature and Water Molar Concentration Measurements Using Thermal and Electrostrictive Laser-Induced Grating Spectroscopy During Operation of a Swirl Burner at Pressure," *J. Eng. Gas Turbines Power* Vol 146 No. 5 (2024): pp. 051021.

[24] Chaib, O., Weller, L., Giles, A., Morris, S., Williams, B. A. and Hochgreb, S. "Spatial Temperature Measurements in a Swirl-Stabilized Hydrogen–Air Non-premixed Flame at Elevated Pressure Using Laser-Induced Grating Spectroscopy," *J. Eng. Gas Turbines Power* Vol 146 No. 11 (2024): pp. 111020

[25] Weller, L., Giles, A., Chaib, O., Morris, S., Williams, B. A. and Hochgreb, S., "Laser induced grating spectroscopy measurements of temperature and water vapour in turbulent lean premixed methane-hydrogen-air flames at pressure," U*nder review*.

[26] Williams, B., Edwards, M., Stone, R., Williams, J. and Ewart, P., "High precision in-cylinder gas thermometry using Laser Induced Gratings: Quantitative measurement of evaporative cooling with gasoline/alcohol blends in a GDI optical engine" *Combustion and Flame* Vol. 161 (2014): pp. 270–279.